Supplementary information for

Temperature-responsive and biocompatible nanocarriers based on clay nanotubes for controlled anti-cancer drug release

Hamoon Hemmatpour[a,b], Vahid Haddadi-Asl[b], Thomas C.Q. Burgers[a], Feng Yan[a], Marc C.A. Stuart[c], Catharina Reker-Smith[d], Rifka Vlijm[a], Anna Salvati[d], and Petra Rudolf[*a]

a Zernike Institute for Advanced Materials, University of Groningen, Nijenborgh 4, 9747AG Groningen, the Netherlands

b Department of Polymer Engineering and Color Technology, Amirkabir University of Technology, P.O. Box 1587-4413, Tehran, Iran

c Electron Microscopy, Groningen Biomolecular Sciences and Biotechnology Institute, University of Groningen, Nijenborgh 7, 9747AG Groningen, The Netherlands

d Department of Nanomedicine & Drug Targeting, Groningen Research Institute of Pharmacy, University of Groningen, A. Deusinglaan 1, Groningen, 9713AV, The Netherlands

Corresponding Author

* Prof. Petra Rudolf

Zernike Institute for Advanced Materials, University of Groningen, Nijenborgh 4, 9747AG Groningen, the Netherlands.

Tel: +(31)50-363 4736, E-mail: p.rudolf@rug.nl

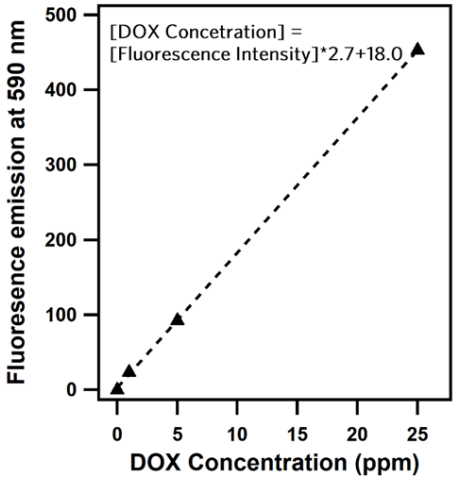

Fig. S1 Calibration curve of DOX fluorescence emission at 590 nm.

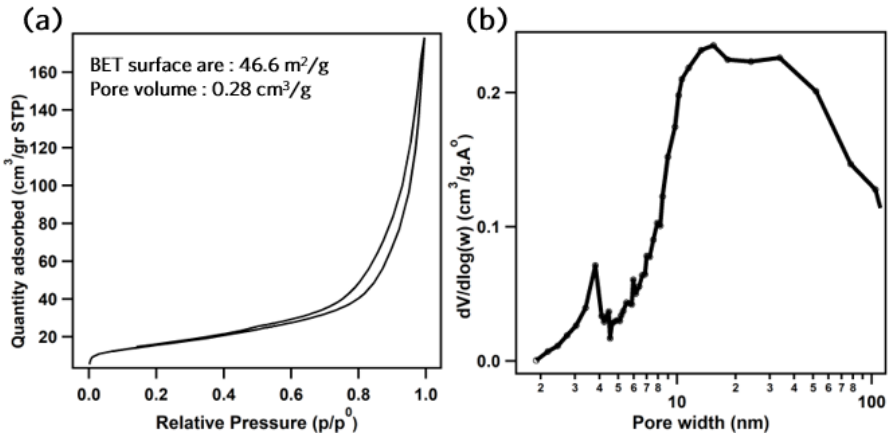

Fig. S2 N2 adsorption/desorption isotherms (a) and Barret-Joyner-Halenda (BJH) pore size distribution (b) of halloysite nanotubes.

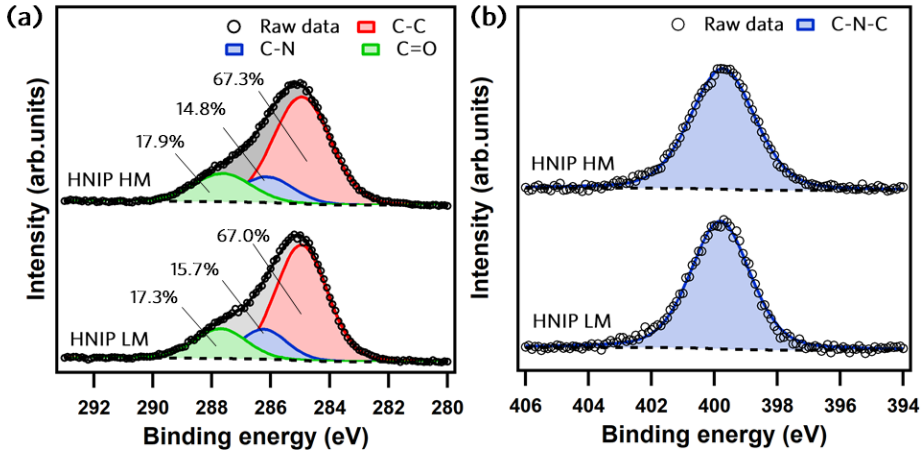

Fig. S3 XPS spectra of the C1s (a) and N1s (b) core level regions of HNIP HM and HNIP LM and corresponding fits.

Calculation of HNTs diameter based on dynamic light scattering analysis

Dynamic light scattering (DLS) is typically used to determine the hydrodynamic diameter (D_h) of the nanoparticles in suspensions. Fig. S4 shows the hydrodynamic diameter distribution and the corresponding average values at various

temperatures for PNIPAM-grafted halloysite nanotubes. For rod-shaped particles the hydrodynamic diameter can be correlated to the length and the diameter of the particles through the following equation:[1-5]

$$d = Le^{(0.32-\frac{L}{D_h})}$$

where D_h (nm) is the hydrodynamic diameter obtained from DLS analysis; L (nm) and d (nm) represent the length and diameter of the particles, respectively. Assuming that the length of the nanotubes remains constant upon heating, the decrease in D_h points to the collapse of the grafted NIPAM brushes. Considering a mean length of 300 nm for the nanotubes based on the TEM image (see Fig. S5), the average diameter of the nanotubes decorated with PNIPM brushes was calculated for each temperature and the results are shown in Fig. 2(d).

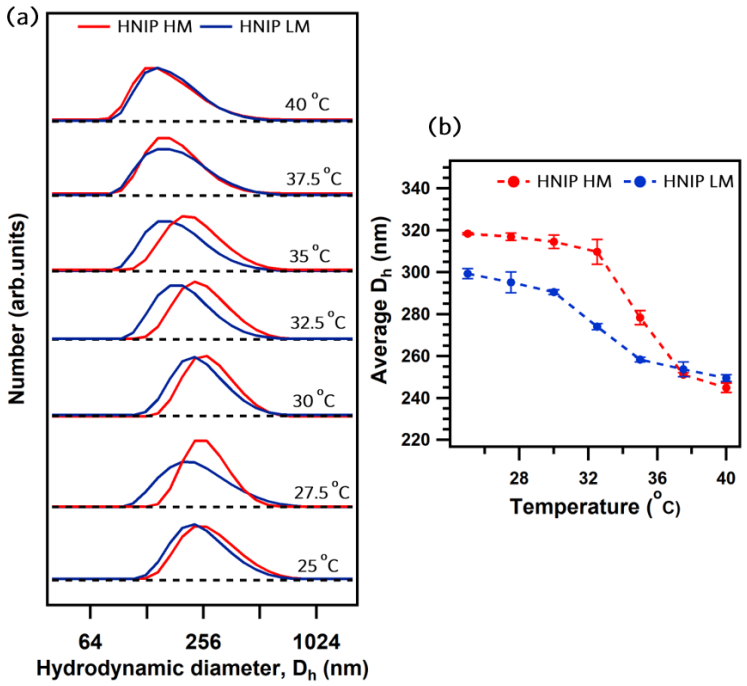

Fig. S4 Hydrodynamic diameter distribution for PNIPAM-grafted halloysite nanotubes (a) and average value of the hydrodynamic diameter (b) at various temperatures.

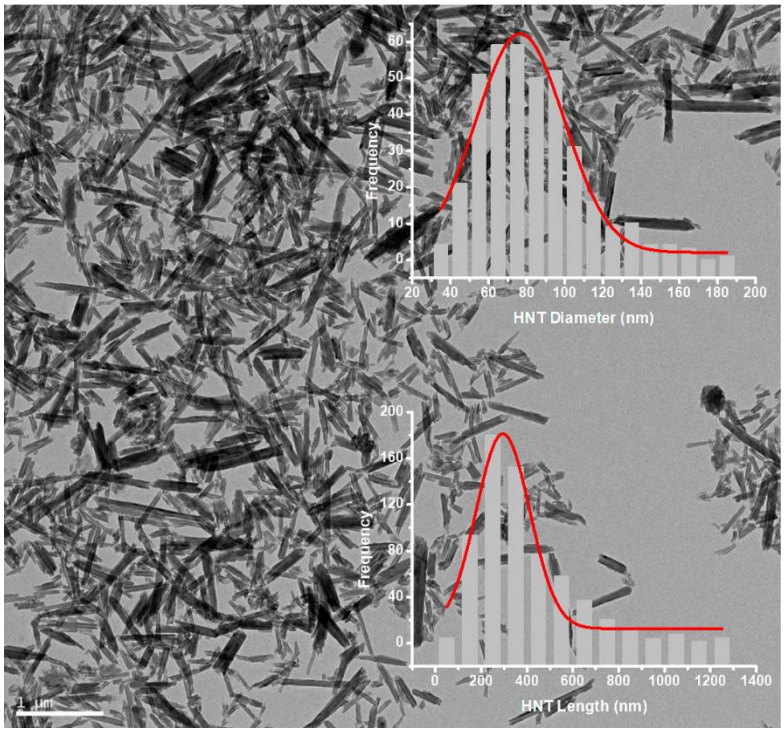

Fig. S5 TEM image of halloysite nanotubes and corresponding length and diameter distribution histograms.

Table S1 Elemental analysis of the PNIPAM-grafted halloysite nanotubes by energy dispersive X-ray spectroscopy.

Sample	Elemental composition (at.%)			
	Si	Al	O	C
HNIP HM	11.8	11.6	58.8	17.7
HNIP LM	13	12.6	61.9	10.2

Table S2 Doxorubicin hydrochloride (DOX) loading capacities for pristine and PNIPAM-grafted halloysite nanotubes.

Sample	Dox loading capacity (mg/mL)
HNT	77
HNIP LM	160
HNIP HM	250

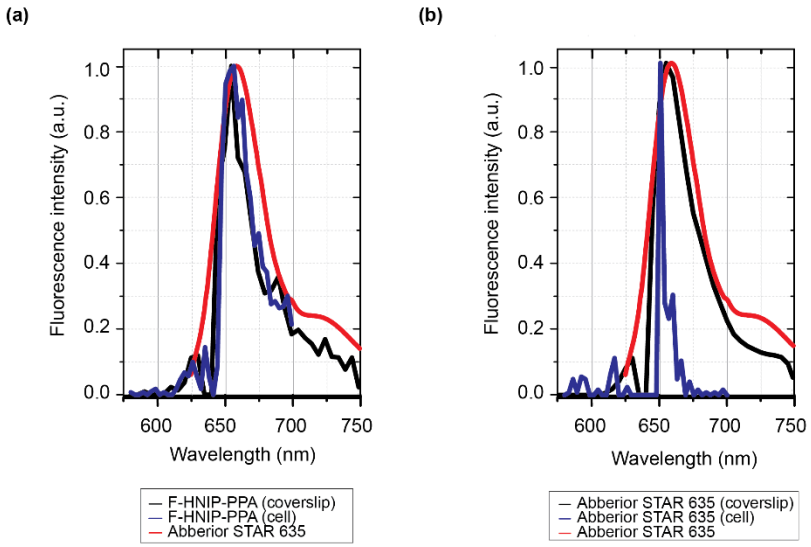

Fig. S6 Comparison of the fluorescence emission spectra of surface-modified halloysite nanotubes functionalized with Abberior STAR 635 dye (F-HNIP-PPA) (a) and the Abberior STAR 635 dye (b). Similar trends are observed when comparing the spectrum as provided by the supplier[6] (red lines) with the signal from F-HNIP-PPA both on a coverslip as well as when taken up by a cell.

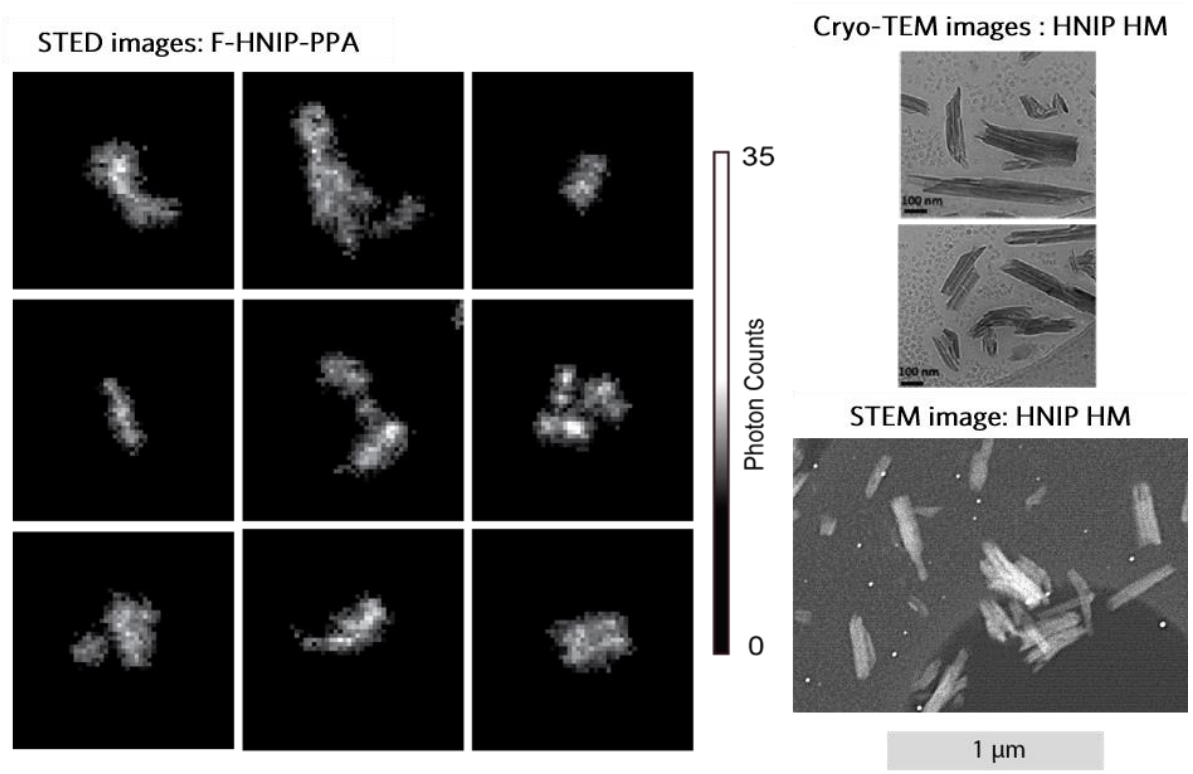

Fig. S7 Fluorescently labeled surface-modified halloysite nanotubes (F-HNIP-PPA, left) compared to the cryo-TEM (right, top) and STEM images (right, bottom). All images have the same scale.

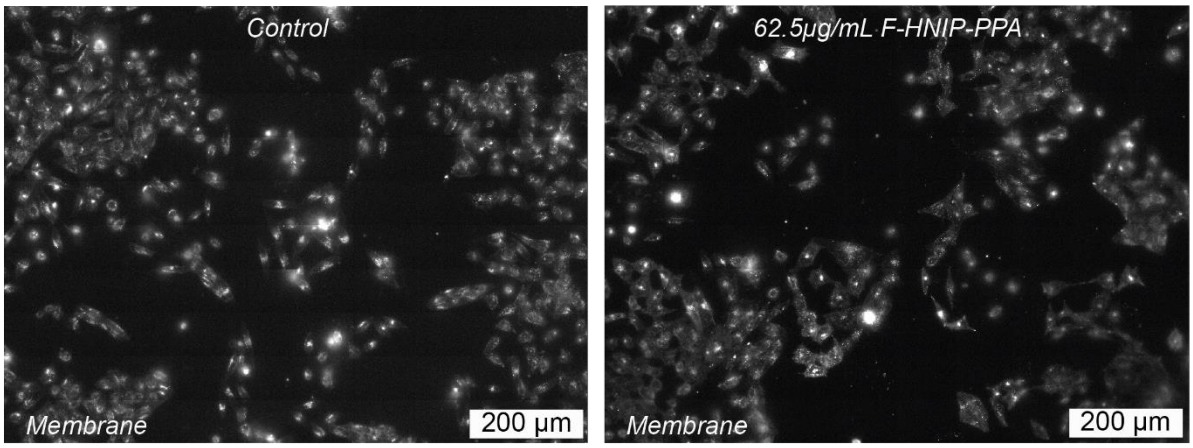

Fig. S8 HeLa cell morphology of cells incubated with 62.5µg/mL F-HNIP-PPA for 48 h versus cells without nanotubes. Rounded cells were quantified, which resulted in 9.3 ± 1.0 % for the control versus 10.3 ± 1.2 % for the cells that were incubated with F-HNIP-PPA, which leads to conclude that there is no significant difference between the two conditions.

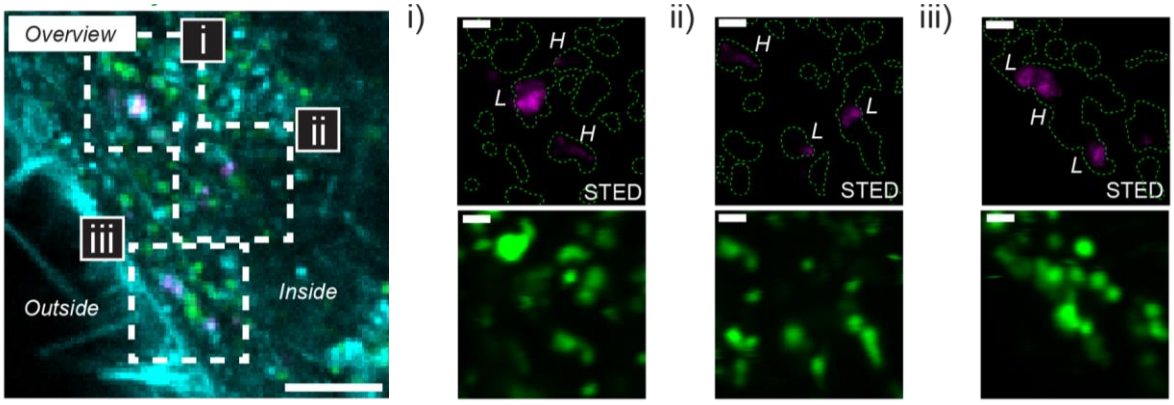

Fig. S9 A cell is displayed showing multiple regions inside the cell where F-HNIP-PPA signal colocalizes with the LysoTracker staining.

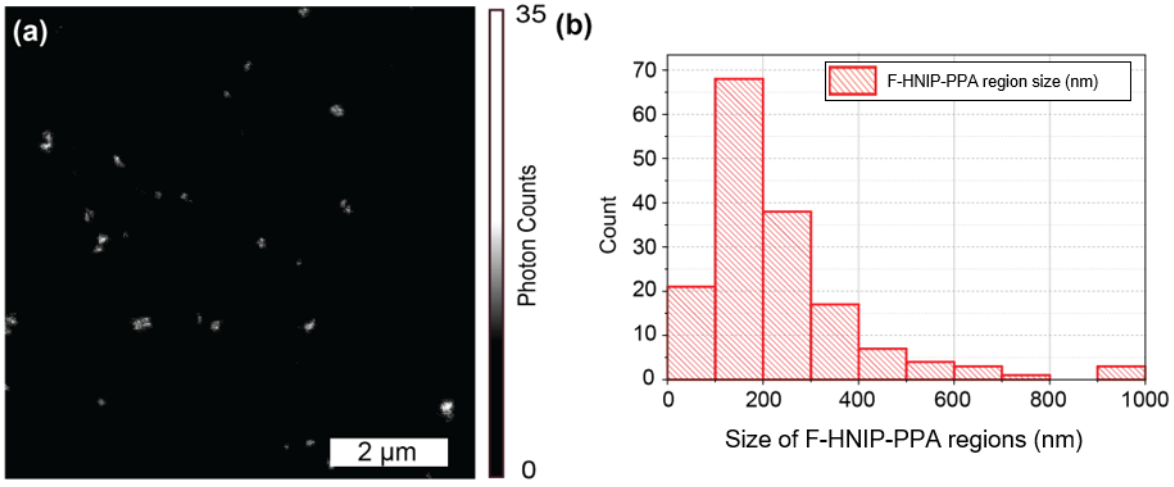

Fig. S10 STED image of the F-HNIP-PPA clusters from a 2.5mg/mL stock solution on a coverslip (a) and an overview of F-HNIP-PPA cluster size distribution (n=3, 156 nanotubes), where the mean was 233 ± 113 nm (b).

References

1. P. Arenas-Guerrero, A. V. Delgado, K. J. Donovan, K. Scott, T. Bellini, F. Mantegazza, M. L. Jiménez, *Scientific Reports,* 2018, ***8*(1)**, 1-10.

2. N. Nair, W. J. Kim, R. D. Braatz, M. S. Strano, *Langmuir*, 2008, **24(5)**, 1790-1795.

3. M. A. Abdulrahaman, O. K. Abubakre, S. A. Abdulkareem, J. O. Tijani, A. Aliyu, A. S. Afolabi, *Advances in Natural Sciences: Nanoscience and Nanotechnology,* 2017, ***8*(1)**, 015016.

4. J. Rodríguez-Fernández, J. Pérez− Juste, L. M. Liz− Marzán, P. R. Lang, *Journal of Phisycal Chemistry C,* 2007, ***111*(13)**, 5020-5025.

5. Malvern Panalytical, Combining Dynamic Light Scattering and Raman Spectroscopy to Characterize Single Wall Carbon Nanotubes (SWNTs). https://www.azonano.com/article.aspx?ArticleID=4133 (accessed 15-09-2022)

6. Abberior https://abberior.shop/abberior-STAR-635 (accessed 10-11-2021).